RESEARCH ARTICLE

Design, synthesis and biological evaluation of light-driven on–off multi-target AChE and MAO-B inhibitors†

Marco Paolino, [iD] *[a] Mariagrazia Rullo, [iD] ‡[b] Samuele Maramai, [iD] ‡[a] Modesto de Candia,[b] Leonardo Pisani, [iD] [b] Marco Catto,[b] Claudia Mugnaini,[a] Antonella Brizzi,[a] Andrea Cappelli, [iD] [a] Massimo Olivucci, [iD] [ac] Federico Corelli [iD] [a] and Cosimo D. Altomare[b]

Neurodegenerative diseases are multifactorial disorders characterized by protein misfolding, oxidative stress, and neuroinflammation, finally resulting in neuronal loss and cognitive dysfunctions. Nowadays, an attractive strategy to improve the classical treatments is the development of multitarget-directed molecules able to synergistically interact with different enzymes and/or receptors. In addition, an interesting tool to refine personalized therapies may arise from the use of bioactive species able to modify their activity as a result of light irradiation. To this aim, we designed and synthesized a small library of cinnamic acid-inspired isomeric compounds with light modulatory activity able to inhibit acetylcholinesterase (AChE) and monoamine oxidase B (MAO-B), with remarkable selectivity over butyrylcholinesterase (BChE) and MAO-A, which have been investigated as the enzyme targets related to Alzheimer's disease (AD). The inhibitory activities were evaluated for the pure E-diastereomers and the E/Z-diastereomer mixtures, obtained upon UV irradiation. Molecular docking studies were carried out to rationalize the differences in the inhibition potency of the E and Z diastereomers of the best performing analogue **1c**. Our preliminary findings may open-up the way for developing innovative multitarget photo-switch drugs against neurodegenerative diseases.

Introduction

Neurodegenerative disorders affect every year an increasing number of people worldwide, especially amongst the elder population, thus representing a substantial economic and social threat in our societies. Different pathological processes contribute to ignite and to advance neurodegeneration, including altered levels of neurotransmitters. Synaptic communication is governed by a fine equilibrium based on the diffusion of small organic molecules able, through the interaction with ligand-gated ion channels and G-protein coupled receptors (GPCR), to switch electrical into chemical signals.[1] A central role is also assigned to carrier proteins and enzymes capable of disposing or inactivating neurotransmitters in the synaptic space.[2] Among the neurotransmitters of greatest interest, acetylcholine (ACh) plays a pivotal role in the stimulation of nicotinic and muscarinic receptors. The concentration of ACh in the synaptic cleft is mainly regulated by the catabolic activity of the enzyme acetylcholine esterase (AChE), which catalyzes the hydrolysis of ACh to acetate and choline, with diffusion-controlled kinetics.[3] Up to date, a large number of AChE inhibitors (AChEIs) has been reported in the literature and some of these agents have found clinical application.[4] One of the most described AChEI, originally approved for the treatment of Alzheimer's disease (AD), is tacrine (Fig. 1), today used only as a research tool, due to its hepatotoxicity.[5,6] Currently approved AChEIs-based therapies (Fig. 1) include rivastigmine (for mild or moderate AD),[7] pyridostigmine (administered orally in the treatment of myasthenia gravis),[8] physostigmine (used in ophthalmology to treat glaucoma),[9] and donepezil (used in humans to treat AD).[10] Worth of note, monoamine oxidase (MAO), a mitochondrial-bound enzyme involved in the oxidation of xenobiotic and endogenous monoamines, is also considered a therapeutic target in various neuropsychiatric and neurodegenerative disorders, such as Parkinson's disease (PD) and AD.[11,12] It exists

[a] Dipartimento di Biotecnologie, Chimica e Farmacia (Dipartimento di Eccellenza 2018-2022), Università degli Studi di Siena, Via A. Moro 2, 53100 Siena, Italy. E-mail: paolino3@unisi.it
[b] Department of Pharmacy-Pharmaceutical Sciences, University of Bari Aldo Moro, Via E. Orabona 4, 70125 Bari, Italy
[c] Chemistry Department, Bowling Green State University, USA
† Electronic supplementary information (ESI) available: ^{1}H and ^{13}C NMR spectra of compounds *E*-**1a–d**; RP-HPLC analytical chromatograms of compounds *E*-**1a–d** and of *Z*-**1c**. See DOI: https://doi.org/10.1039/d2md00042c
‡ These authors contributed equally.
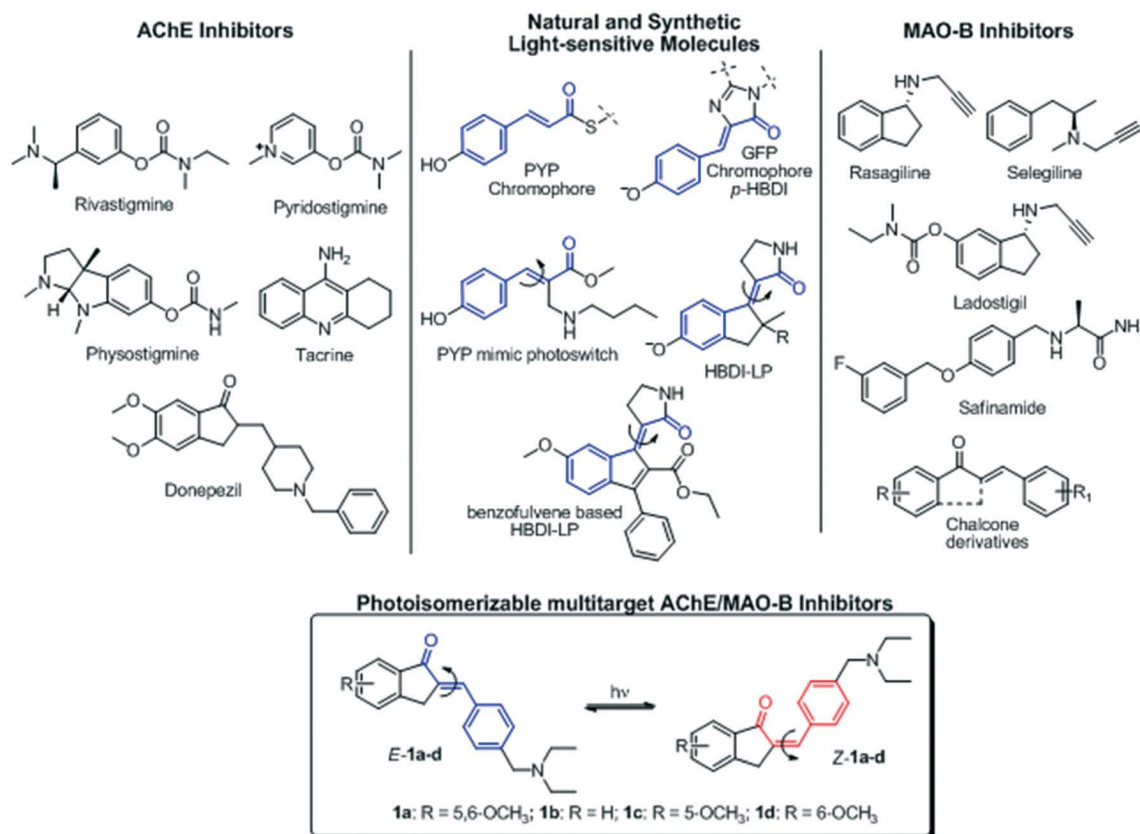
Fig. 1 Comparison of the structures of AChE and MAO–B inhibitors and of natural and synthetic light–sensitive chromophores considered for the design of photoisomerizable multitarget AChE/MAO–B inhibitors reported in the present article.

in two different isoforms, MAO-A and MAO-B, demonstrating significant sequence similarity but differing in their substrate recognition and tissue distribution.[13] The oxidation process catalyzed by MAO results in the formation of reactive oxygen species (ROS) as by-products, which might cause oxidative damage in brain tissues. Therefore, inhibitors of MAO enzymes have the potential to reduce oxidative stress and to enhance monoamine neurotransmitter effects in the CNS.[14] MAO-B selective and reversible/irreversible inhibitors have demonstrated broader therapeutic effects, such as neuroprotection and cognitive improvement.[11,13] Rasagiline, selegiline, and safinamide (Fig. 1) have already been approved for the treatment of PD,[15] while interesting chalcone derivatives (or masked chalcone derivatives), displaying similar activities, have been reported in the literature.[16–18] Owing to the fact that neurodegenerative disorders represent complex and multifaceted diseases resulting from the co-subsistence of different pathological factors, the strategy of finding a multi-target-directed ligand (MTDL), hitting more than a single target at the same time, has been the focus of the most promising researches in the last decade.[19–22] Interestingly, ladostigil, a dual inhibitor of AChE and MAO-B, advanced in phase II clinical trial for AD (NCT01354691).[23] Therefore, there is a great potential for novel agents targeting AChE and MAO-B to be useful tools for the development of future therapies against neurodegenerative diseases. The pharmacological research on

AChE and MAO inhibitors has made a huge step forward, but the search for innovative and precise pharmacological agents with high affinity and selectivity that can be reversibly modulated is still challenging.

Different approaches based on external stimuli have been used to generate bioactive species in specific compartments of the human body. Among these, in the last decade a growing interest has been directed towards the photopharmacology approach based on the use of bioactive molecules that change their effectiveness towards their target(s) as a result of irradiation with light.[24] In principle, the use of light offers several advantages, as light is not invasive, does not contaminate the biological environment, has limited (if not zero) toxicity, and can be controlled with very high spatial and temporal precision.[24] The development of molecules for photopharmacology is mainly based on two strategies: 1) conjugation of the bioactive species with a photolabile inactivating group that can be removed *in situ* by light irradiation. This leads to high concentration of the active compound in the irradiated site, which subsequently and irreversibly follows its pharmacokinetic path;[25] 2) conjugation of the bioactive molecule with well-known molecular photo-switches, first of all azobenzene.[25–27] The photoinduced change produces variations in the geometry, polarity, and spatial position of functional groups by modulating the affinity of the compound for the target binding site. The photoisomerizable

accessory fragments allow the bioactive species to be reversibly activated and/or deactivated, simply by modulating the power and wavelength of the light source used. However, this conjugation often results in a significant loss of activity in the final structure.[24–27]

The literature of the last 10 years has proposed the photopharmacological approach for the control of ion channels,[28–30] enzymes[31,32] and GPCRs.[26,27,33] Furthermore, examples (mainly based on azobenzene photoswitch) have been given regarding AChE or its isoform BChE,[34–37] while no interest has been paid to MAO-B. Given their role in the neuronal network performed with extremely rapid kinetics, it would be desirable to obtain valid ultrafast dual photomodulating tools.

Recently, some of us have been involved in the design of new light driven molecular switches (LDMS) using the so called "biomimetic strategy". In particular, we reported the synthesis and characterization of neutral or negatively charged compounds based on the transformation of the green fluorescent protein fluorophore (*i.e. p*-HBDI, Fig. 1) from an efficient emitter into a molecular photoswitch (*i.e.* HBDI-LPs and benzofulvene-based HBDI-LP, Fig. 1)[38,39] and of a *p*-hydroxycinnamate analogue of the photoactive yellow protein (PYP) chromophore structure.[40] The HBDI-LPs perform the *E/Z* photoisomerization with relatively high isomerization quantum yield in picosecond and sub-picosecond timescale under UV/vis light irradiation.[38,39] These molecules share the common feature of an electron-rich group conjugated to an electron-withdrawing group by means of an isomerizable carbon–carbon double bond, in order to generate push–pull cinnamic structures. The photoisomerization of these asymmetric systems leads to a spatial reposition of functional groups that can be exploited to generate new intra- and intermolecular interactions.

In this work, we present the first results of our research on the push–pull cinnamic fragment research, which we consider the cornerstone of our biomimetic molecular photointerrupters. These studies also paved the way for the identification and optimization of bioactive compounds with light modulatory activity. As anticipated, our attention has focused on the AChE and MAO-B enzymes. Starting from the cinnamic fragment masked in AChEI **1a** (structurally related to the selective AChEI donepezil, Fig. 1) already reported as *E* diastereomer by Sheng *et al.*[41–45] and similarly found in other MAO-B inhibitors,[16–18] we synthesized a small series of compounds (**1a–d**, Fig. 1 and Scheme 1) that differ in the presence or position of the methoxy auxochrome group, and

we evaluated their propensity to the isomerization as a result of irradiation with UV-B light. For each compound, the inhibitory activity on AChE of both the pure *E*-diastereomer and the *E/Z*-diastereomer mixture obtained upon reaching the photostationary state (PSS) was evaluated. As a further step, MAO (both A and B isoforms) inhibitory activity was evaluated for each pure *E*-diastereomer and for the *E/Z*-diastereomer mixture of the most promising (in terms of combined biological and photophysical properties) compound **1c**. Finally, the differences in inhibition activity were rationalized based on molecular docking studies.
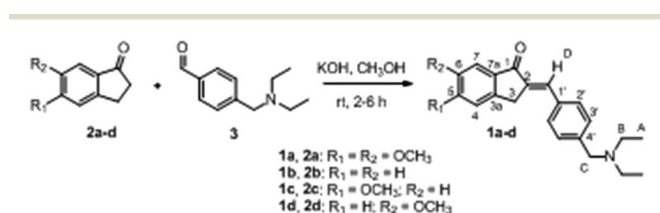
Results and discussion

Design and synthesis

The presence in compound **1a** of a single exocyclic double bond that conjugates an aromatic ring to a carbonyl group entrapped in a masked chalcone structure makes this molecule an excellent starting point for the development of photoisomerizable multitarget AChE and MAO-B inhibitors. This compound, reported as *E*-diastereomer by Sheng *et al.*,[41] has excellent inhibitory activity on AChE (IC$_{50}$ of 35 nM on rat AChE) and remarkable selectivity (IC$_{50}$ BChE/AChE ratio <1000),[41] while analogue indanone derivatives show activity against MAO-B in the submicromolar range.[17,46]

Furthermore, the presence of methoxy groups on the indole ring, similarly to donepezil, could in principle be used to modulate the photophysical and photochemical properties; accordingly, they were varied in the new compounds **1b–d** in order to explore the chemical space available to obtain good pharmacological and optical properties.

Compounds **1a–d** were obtained by aldol condensation of 4-(diethylaminomethyl)benzaldehyde (**3**) with the appropriate indanone **2a–d** using KOH in methanol as shown in Scheme 1. All compounds were isolated as a single diastereomer, which *E*-geometry was assigned by NMR studies. In particular, ^{1}H–^{1}H NOE experiments showed contacts between H-2′ and H-3 (see Scheme 1 for the numbering). Moreover, in the ^{1}H NMR spectrum of all the compounds **1a–d** the vinyl proton (D) shows a chemical shift around 7.5 ppm compatible with the deshielding effect exerted by the carbonyl group.

Photophysical and photochemical features of the chromophore

The initial photophysical and photochemical characterization focused on the *E*-diastereomers of compounds **1a–d**. Their absorption spectra registered in methanol at concentrations compatible with the UV-vis spectroscopy (about 10^{-5} M) (Fig. 2) are dominated by an intense peak with an absorption maximum dependent on the number and position of the methoxy groups of the indanone aromatic ring. In particular, the absence of methoxy groups (compound **1b**) gives rise to an absorption maximum centered at 327 nm, while the presence of one methoxy group in position 5 (compound **1c**) causes a red-shift at 333 nm. When the methoxy group is located in position 6 of the indanone scaffold (as in

Scheme 1 Synthesis of compounds *E*-**1a–d**.

1a, 2a: R$_1$ = R$_2$ = OCH$_3$
1b, 2b: R$_1$ = R$_2$ = H
1c, 2c: R$_1$ = OCH$_3$; R$_2$ = H
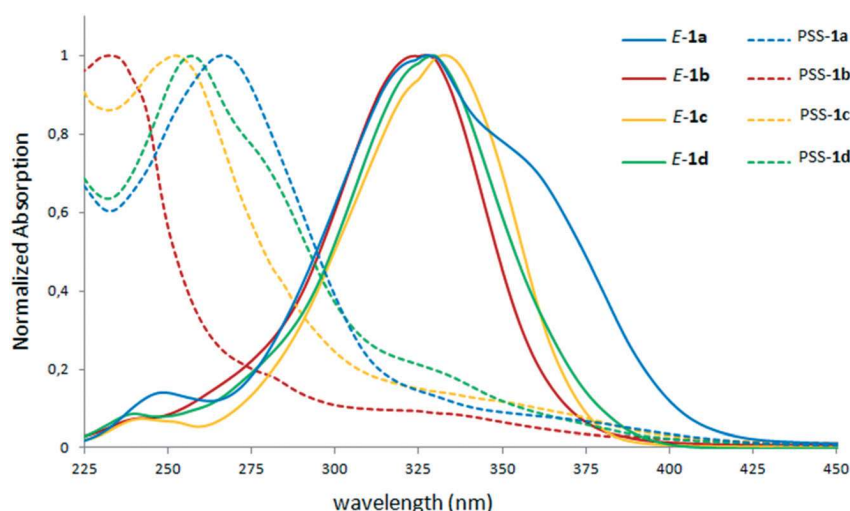**1d, 2d:** R$_1$ = H; R$_2$ = OCH$_3$

Fig. 2 Normalized UV–vis absorption spectra of methanolic solution of compound **1a–d** (solid lines) and the same solution after irradiation until PSS with UV–B light source (dotted lines).

compound **1d**) the absorption maximum shift at 330 nm. The simultaneous presence of two methoxy groups, as in compound **1a**, produces an absorption spectrum consisting of a main band at 328 nm, accompanied by an intense shoulder at about 360 nm. The presence of the latter generates an absorption tail up to about 410 nm, missing in the other compounds, which show an absorption tail up to about 390 nm. Interestingly, the absorption spectrum of these molecules largely overlaps the emission spectrum of UV–B lamps, commonly used in photochemistry laboratories. Therefore, the photoisomerization of compounds **1a–d** was performed using this light source, with the aim of photoinducing the formation of the Z-diastereomers.

The irradiation of each solution up to the photostationary spectrum causes a drastic reduction of the absorption bands attributed to the E-diastereomers and the appearance of new blue-shifted absorption bands whose absorption maximum changes depending on the presence and number of methoxy groups on the indanone scaffold. This blue-shift effect is in line with what has been reported in the literature as reduction of the π–π electron conjugation during the formation of the Z-isomer of many analogue chromophores, including coumarin and cinnamic, ferulic, and caffeic acids.[47] In order to monitor and quantify the photoinduced formation of the Z-diastereomer, the photoisomerization behaviour of **1a–d** was evaluated by NMR spectroscopy. NMR experiments were performed into Pyrex NMR tubes at room temperature by irradiating concentrated solution (from 1 mM up to 10 mM) with UV–B light source.

After irradiation at these concentrations, a pale-yellow solution with a white precipitate formed in all the samples. ^{1}H and ^{13}C NMR spectra of each compound revealed the presence in solution of an apparent PSS (generated by light irradiation and governed by solubility) constituted of the E-diastereomer together with its Z-isomer (identified by homonuclear ^{1}H–^{1}H-NOESY, and heteronuclear ^{1}H–^{13}C-

HSQC, ^{1}H–^{13}C-HMBC 2D correlation experiments). The diastereomeric ratio of the obtained **1a–d** apparent PSS was determined by computing the area of the well distinguishable signals assigned to E- and Z-isomer in the ^{1}H NMR spectra (Fig. 3). In particular, an apparent PSS consisting of 75% of the Z-diastereomer was observed with compounds **1b**, **c**, while the Z-diastereomer represents the 65% and 45% of the mixture in compound **1d** and **1a**, respectively. The dissolution of the precipitates by addition of DMSO-d$_6$ reveals a slight increase in the Z-diastereomer for each compound.

In order to evaluate the possibility to photochemically convert the Z-diastereomers into the E-diastereomers, the PPS mixture of compound **1c**, obtained by irradiation with UV–B light, was again irradiated with UV–C lamps in a quartz cuvette. After 1 hour of irradiation a partial interconversion of Z-**1c** into E-**1c** was obtained, in line with what has been reported in the literature for similar scaffolds.[48] However, due to the high energy of this light, prolonged exposure to UV–C light causes photochemical degradation.

The thermal stability of Z-**1c** was evaluated by observing the E/Z interconversion via ^{1}H NMR analysis. Solutions at PPS$_{UV-B}$ stored in the dark (or even exposed to visible ambient light not absorbed by the compounds) were monitored for 12 days at room temperature and at 50 °C. The kinetic experiments revealed a high thermal stability of the photoinduced Z-diastereomer that very slowly interconverts in the E-diastereomer without decomposition with an estimated half-life in methanol solution of about 47 days at room temperature and 26 days at 50 °C (see ESI†).

Biological evaluation

After filtration, the clear methanolic solutions of compounds **1a–d** monitored by NMR spectroscopy were concentrated under a gentle nitrogen stream. The resulting solid materials (constituted of a well-known E/Z ratio) and the pure E
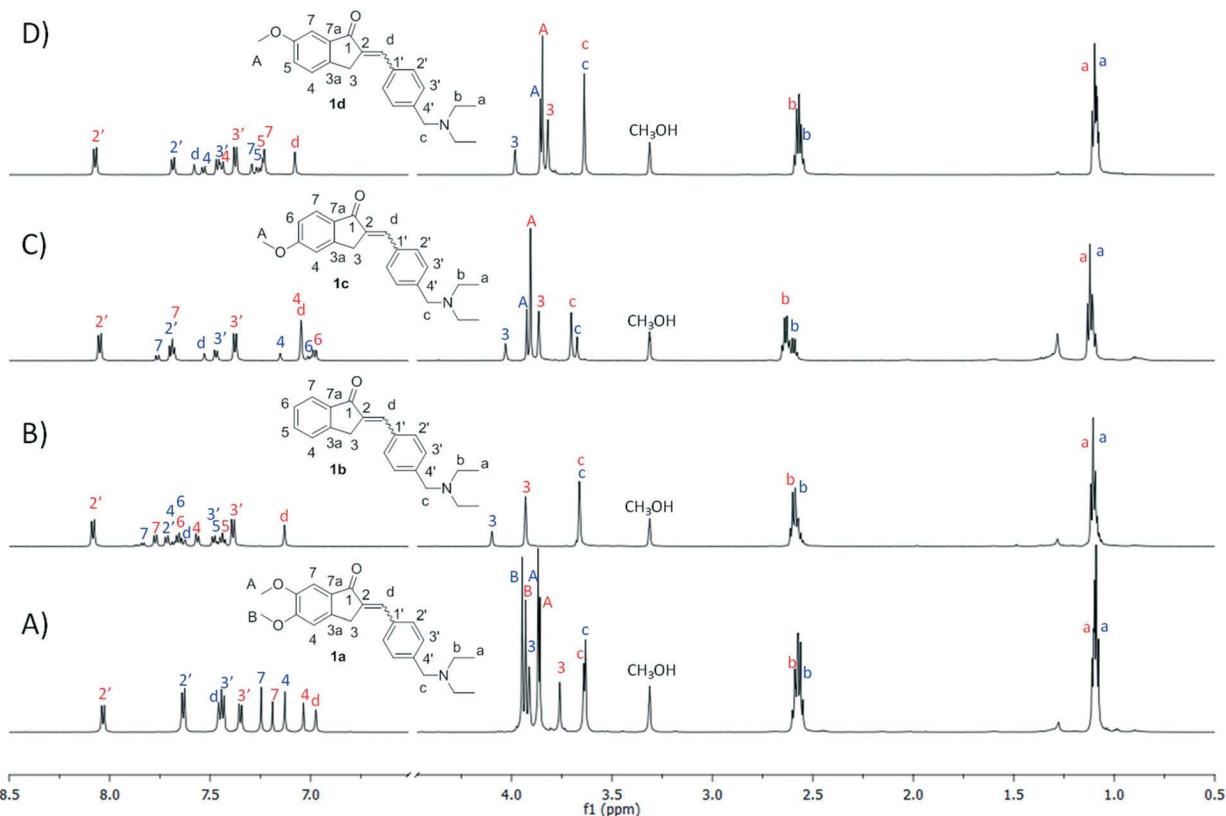
Q4 **Fig. 3** ^{1}H NMR spectra (methanol-d_4, 600 MHz) of the diastereomeric mixtures of compounds **1a–d** at the apparent PSSs obtained by irradiation with UV–B light. Blue numbering has been used for the *E*-diastereomers (red numbering for the *Z*-diastereomers).

diastereomers were evaluated for their inhibition potency against human ChEs isoforms (AChE and pseudocholinesterase butyryl, BChE), and MAO (A and B isoforms).

ChEs inhibitory activities were tested using the Ellman's assay, with slight modifications.[49] In these experiments, **1a** achieved inhibition of human AChE at concentrations slightly higher than those previously determined by others on rat cortex homogenates,[41] while all the compounds tested herein showed weak inhibition of BChE.

The position of the methoxy groups affected AChE inhibition potency. The mono-substituted derivatives **1c** and **1d**, bearing 5-OCH$_3$ and 6-OCH$_3$, respectively, and the unsubstituted congener **1b** as well, proved to be less active than **1a**. The inhibition data suggest that a main contribution to anti-AChE potency comes in particular from the 5-OCH$_3$ group. Compound **1c** showed a potency only two times lower than **1a**. In contrast, the 6-OCH$_3$ derivative **1d** resulted less potent than both **1b** and **1c**. It can be inferred that methoxy group at C6 may improve the binding in the AChE active site only in cooperation with another methoxy *ortho*-positioned at C5, whilst it appeared unfavorable when alone.

MAO-A/B inhibition was also determined for pure *E* isomers, based on some literature findings for close structural congeners.[17,46] We disclosed inhibitory potencies in the submicromolar range and notable selectivity toward the MAO-B isoform, thus confirming the potential of this

class of compounds as multitarget agents for neurodegenerative disorders. A valuable exception was represented by **1d**, acting as a very potent, yet unselective, inhibitor of both A and B isoforms, with IC$_{50}$ equal to 95 and 91 nM, respectively. Even in the case of MAO inhibition, the effects of methoxy group seem strongly dependent on the substitution position, but with different trends than AChE inhibition. The 6-methoxy derivative **1d** (the less active AChEI) is the most potent inhibitor, whereas **1a** (the most potent AChEI) is the less active MAO-B inhibitor. On the other hand, although the fact that compound **1c** does not show the best activity on AChE and MAO-B among the compounds of the series, it seems to have the best biological profile with a moderate inhibitory capacity in the submicromolar range on both enzymes and excellent selectivity towards their isoforms.

All the tested *E/Z* mixtures were found to be less active than the corresponding *E* isomers, indicating that the *Z* isomers possess a lower binding affinity toward AChE compared to the *E* isomers. To corroborate this finding, the *E/Z* mixture of compound **1c** was resolved by RP-HPLC separation.[50] The isolated *Z*-**1c** was then assayed resulting one order of magnitude less active than the corresponding *E* isomer in both AChE and MAO-B inhibition.

Finally, the compounds were tested for their potential in inhibiting the spontaneous aggregation of Aβ$_{40}$, the protein

responsible for the accumulation of extracellular insoluble aggregates known as senile plaques in the AD brain. The inhibition of amyloid aggregation, supporting the so-called amyloid hypothesis in AD insurgence, is still a pursued target despite many failures of antiamyloid agents in clinical trials.[51] In our *in vitro* assay, the *E/Z* mixtures were tested at a concentration of 100 μM to reveal any putative activity to be further evaluated on pure *E* isomers. As listed in Table 1, no appreciable inhibition of Aβ$_{40}$ aggregation was found, except for **1a**, whose 5,6-dimethoxyindane structure represents a known scaffold for efficient disruption of protein aggregation.[52]

Molecular docking simulations

Aiming at investigating the effect of the double bond geometry on the enzymes' inhibitory potencies at the molecular level, the analogue **1c**, which achieved the best balance in terms of AChE and MAO-B IC$_{50}$s as pure *E* diastereomer, was studied by molecular docking simulations into the binding site of the two enzymes. At first, the docking of both **1c** diastereoisomers to the crystal structure of binary AChE complex with donepezil (PDB entry 4EY7) was assessed *in silico*. As inferred by Fig. 4, the (*E*)-geometry of the exocyclic double bond allowed a better three-dimensional overlap between the skeleton of donepezil and compound *E*-**1c** than *Z*-**1c**. In its top-scored binding pose, the inhibitor was fully buried in the active site, occupying the gorge from PAS to CAS. In both donepezil and *E*-**1c** complexes, the indanone core was packed against W286 within PAS through a parallel-displaced arene–arene interaction. The carbonyl groups pointed toward F295, further stabilizing the binding with a hydrogen bond to backbone NH. Thanks to a proper alignment in the region surrounding CAS, the protonatable nitrogen atom of the inhibitor was involved in a cation–π

interaction with W86, thus matching the π–π stacking returned by donepezil. Fig. 4B displayed the binding pose of *Z*-diastereomer. At first sight, in its top-ranked bound conformation the inhibitor lost the planar topology to unburden steric clashes. Close contacts with W86 (cation–π interaction with N) and W286 (π–π stacking with indanone) were preserved, whereas the phenyl ring was accommodated in a cage lined by aromatic side chains (Y341, F338, Y124). The indanone nucleus was rotated by 180°, which prevented the correct hydrogen bonding positioning of C=O in front of F295 (NH$_{backbone}$).

Moreover, the X-ray structure of MAO-B complexed with safinamide was retrieved from PDB (entry 2V5Z) and employed to dock the most potent MAO-B diastereomer *E*-**1c** in order to postulate reliable binding poses toward this target. As shown in Fig. 5, the compound was lodged within the substrate cavity by orienting the indanone core toward FAD coenzyme. Two π–π interactions anchored the bicyclic scaffold and the phenyl linker to Y398 and Y326, respectively, whereas a hydrogen bond was directed to 5-methoxy substituent from Y188 side chain. Docking simulations of *E*-**1c** with the crystal structure of MAO-A complexed with harmine (entry 2Z5X) were performed to possibly reveal the molecular factors likely related to the MAO-isoform selectivity (the selectivity ratio toward the B-isoform was higher than 40). As shown in Fig. 5B, the lower inhibitory potency of *E*-**1c** toward MAO-A could be ascribed to steric hindrance between the *N*-diethyl benzylamine moiety of *E*-**1c** and the gate-keeper residues I335 and F208.

Conclusions and perspectives

In conclusion, a small series of compounds (**1a–d**) was designed and synthesized combining the structural properties

Q5 Table 1 Half maximal inhibitory concentration (IC$_{50}$) values (μM) of human cholinesterases (AChE and BChE) and monoamine oxidases (A and B), and % inhibition of Aβ$_{40}$ self aggregation

| cmpd[a] | IC$_{50}$(μM) or % inhibition at 10 μM | | | | |
	AChE[b]	BChE[b]	MAO-A	MAO-B	Aβ$_{40}$ aggr.[c]
E-**1a**	0.063 ± 0.001	n.a.	(49.6% ± 3.3)	0.783 ± 0.095	n.t.
E/Z-**1a** (55/45)	0.253 ±0.001	n.a.	n.t.	n.t.	56.0% ± 3.2
E-**1b**	0.612 ± 0.069	(17.8% ± 1.1)	(42.7% ± 1.3)	0.661 ± 0.042	n.t.
E/Z-**1b** (25/75)	1.31 ± 0.41	(16.2% ± 2.2)	n.t.	n.t	8.1% ± 4.7
E-**1c**	0.113 ± 0.001	n.a.	(32.8% ± 2.9)	0.260 ± 0.012	7.4% ± 5.0
E/Z-**1c** (25/75)	0.505 ± 0.062	n.a.	(45.1% ± 4.8)	1.59 ± 0.04	n.t.
Z-**1c**	1.15 ± 0.11	n.a.	(28.2% ± 3.7)	1.94 ± 0.04	23.4% ± 2.3
E-**1d**	0.964 ± 0.004	(14.3% ± 2.1)	0.095 ± 0.025	0.091 ± 0.004	n.t.
E/Z-**1d** (35/65)	1.10 ± 0.12	(8.3% ± 1.3)	n.t.	n.t.	37.7% ± 2.2
Donepezil	0.017 ± 0.002	4.80 ± 1.00	—	—	—
Tacrine	0.093 ± 0.005	0.024 ± 0.001	—	—	—
Safinamide	—	—	(18.2% ± 3.0)	0.029 ± 0.002	—
Quercetin	—	—	—	—	84.4% ± 7.2

[a] For *E/Z* mixture the diastereomeric composition determined by ^{1}H NMR spectroscopy is reported in the brackets. [b] Human cholinesterases. IC$_{50}$ values determined by interpolation of the sigmoidal dose–response curves as obtained by regression with GraphPad Prism software (ver. 5.01), of at least seven data points, or inhibition percentage at 10 μM concentration in parentheses; n.a. = not active, n.t. = not tested. Data are means ± SD of three independent measurements. Donepezil, and tacrine were used as positive controls. [c] Human recombinant MAOs. Safinamide was used as positive control. [d] Percent of inhibition of Aβ$_{40}$ self-aggregation at 100 μM concentration. Data are mean ± SD of three independent measurements; quercetin was used as positive control.
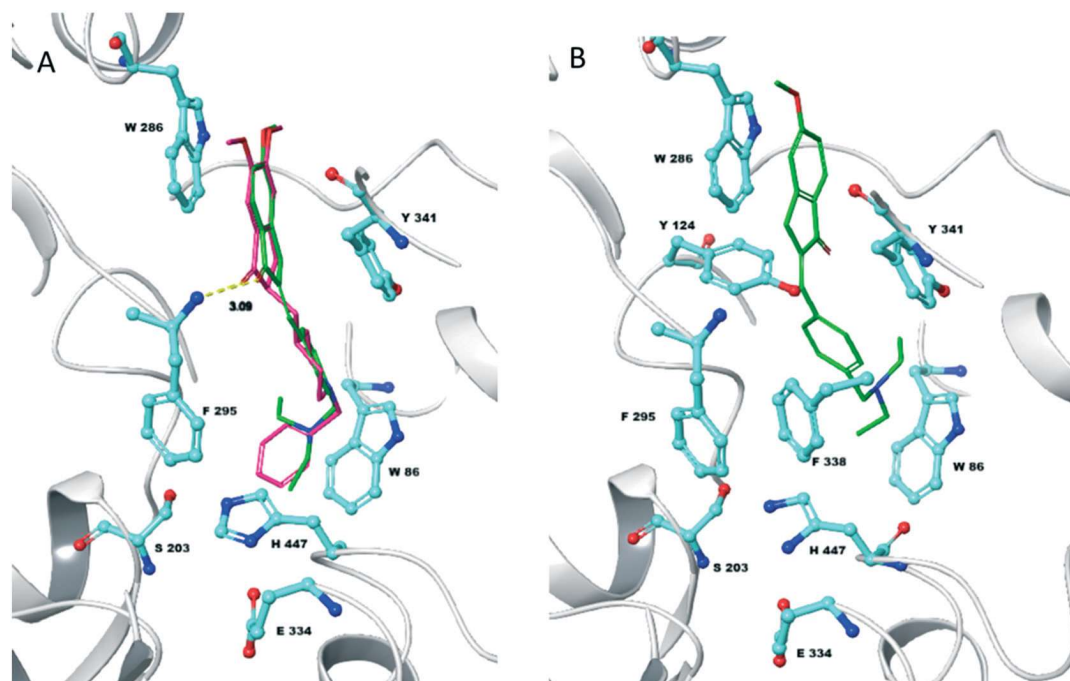
Fig. 4 Top-scored docking poses of compounds *E*-**1c**, *Z*-**1c** and donepezil in complex with *h*AChE (PDB 4EY7). Ligand is rendered as sticks, relevant amino acid residues are rendered as ball-and-sticks, while protein is represented as a cartoon. Colours are in according to the atom code, C atoms in cyan and green (or magenta) for amino acid and ligand, respectively. Dotted lines represent H-bond. A) Superimposition of *E*-**1c** (green, docking score −12.06 kcal mol^{-1}) and donepezil (magenta, docking score −12.51 kcal mol^{-1}). B) Top-ranked docking pose of *Z*-**1c** (green, docking score −10.33 kcal mol^{-1}).
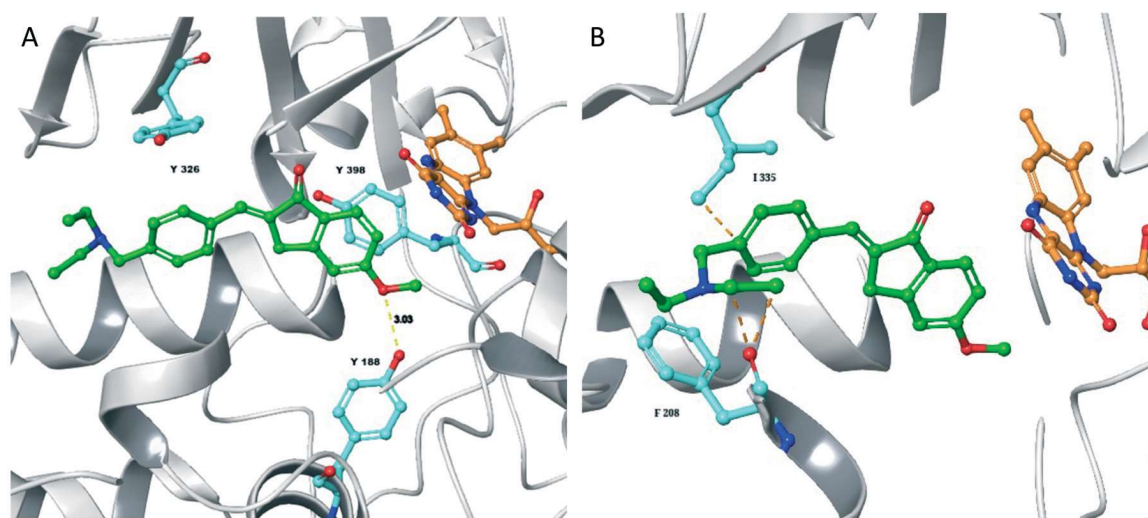
Fig. 5 Top-scored docking poses of compound *E*-**1c** with: A) *h*MAO-B (PDB 2V5Z) (docking score −10.86 kcal mol^{-1}) and B) *h*MAO-A (PDB 2Z5X) (docking score −10.02 kcal mol^{-1}). Ligand and relevant amino acid residues are rendered as ball-and-sticks, while proteins are represented as cartoons. Colors are in according to the atom type, C atoms in cyan and green for amino acids and ligand, respectively; FAD coenzyme in orange. Yellow dotted lines represent H-bonds; orange dotted lines indicate possible steric clashes.

of biomimetic molecular photoswitches and inhibitors of two well-studied enzymes involved in neurodegenerative diseases, namely AChE and MAO-B. The new compounds, bearing an exocyclic double bond involved in a push–pull type structure, were characterized from a photochemical point of view in order to explore their ability to act as LDMS. In accordance with their UV-vis spectra, UV-B light irradiation of the molecules in solution gives rise to interconversion of the *E*- into the *Z*-diastereomer without promoting any degradation during the photoreaction. The inhibitory activity of the synthesized compounds as *E*-diastereomers was tested on both AChE and MAO-B as well as on their major isoforms (BChE and MAO-A).

Pure *E* diastereomers revealed interesting inhibitory potencies against both enzymes in the submicromolar range modulated by the presence of the methoxy groups. Notably, compound **1c**, bearing only the 5-methoxy group, possesses the most interesting biological profile, showing good inhibitory capacity in the submicromolar range on both enzymes (AChE IC$_{50}$ = 0.113 μM, MAO-B IC$_{50}$ = 0.26 μM), with high isoform selectivity.

The UV-B light irradiation of the *E*-diastereomers produced *E*/*Z* mixtures which elicited decreased activity on AChE suggesting a lower binding affinity for the *Z* isomers. The resolution by RP-HPLC of the *E*/*Z*-mixture of the most promising compound **1c** confirmed our hypothesis, revealing a decreased potency of one order of magnitude for *Z*-**1c** compared to *E*-**1c** towards both enzymes.

Molecular docking studies performed on compound **1c** helped rationalizing the differences in the inhibition potency of the two diastereomers, mainly driven by different interaction patterns with the aminoacidic residues in the enzymatic pockets.

These results highlight an off-activity behavior after UV-B light irradiation that can potentially be restored using appropriate blue-shifted wavelengths and put in evidence a first prototype of multi-target-directed pharmacological tool with photomodulated activity for neurodegenerative diseases models. Accordingly, our research activity will continue by combining computational, synthetic and biological efforts, in order to achieve second generation molecules with improved characteristics, both in terms of optical (*e.g.*, molecules with red-shifted absorption spectra) and pharmacological (*e.g.*, increased inhibitory potency, drug-likeness) profiles for application in *ex vivo* and *in vivo* models.

Experimental section

Materials and methods

Synthesis. All chemicals used were of reagent grade. Yields refer to purified products and are not optimized. Merck silica gel 60 (230–400 mesh) was used for column chromatography. Merck TLC plates and silica gel 60 F$_{254}$ were used for TLC. NMR spectra were obtained with a Bruker 400 and 600 AVANCE spectrometer in the indicated solvents. The chemical shifts are referenced to the residual not deuterated solvent signal (CHD$_2$OD: δ(^{1}H) = 3.31 ppm, δ(^{13}C) = 49.86 ppm). The values of the chemical shifts are expressed in ppm and the coupling constants (*J*) in Hz. An Agilent 1100 LC/MSD operating with an electrospray source was used in mass spectrometry experiments. Purity of compounds **1a–d** was assessed by RP-HPLC (Agilent 1100 series) and was found to be higher than 95%. Zorbax Eclipse XDB-C8 column (4.6 × 150 mm, 5 μm) was used in the HPLC analysis with methanol–H$_2$O (0.1% formic acid) (80:20) as the mobile phase at a flow rate of 0.5 mL min^{-1}. UV detection was achieved at 280 nm. The absorption spectra were recorded with a PerkinElmer Lambda 40 in the indicated solvent. Compound **3** was prepared as reported in ref. 53. UV-B and UV-C irradiations were conducted using a Multyrays chamber

equipped with 2 G15T8 Hg UV-B tube (2 × 15 Watt) or 2 G15T8 Hg UV-C tube (2 × 15 Watt) in continuous rotation.

General procedure for the synthesis of compounds 1a–d. Compounds **1a–d** were prepared by optimizing a procedure reported in ref. 41. To a solution of KOH (0.046 g, 0.82 mmol) in 20 mL of methanol, aldehyde **3** (0.11 g, 0.575 mmol) and the appropriate indanone (0.55 mmol) were added. The resulting mixture was stirred at room temperature under nitrogen atmosphere for 6 h. Subsequently, the solvent was removed under reduced pressure to obtain an oily residue, which was dissolved in ethyl acetate and washed with brine. The organic phase was dried over anhydrous sodium sulfate, filtered, and concentrated under reduced pressure. The residue was purified by flash chromatography with ethyl acetate/methanol (9:1) as the eluent to afford an off-white solid corresponding to the desired compound **1a–d** as *E* diastereomer. NMR data of the *Z* diastereomers of each compound were derived after UV-B light irradiation of the corresponding *E* diastereomer until the apparent PSS.

(***E***)-2-(4-((Diethylamino)methyl)benzylidene)-5,6-dimethoxy-2,3-dihydro-1*H*-inden-1-one (***E***-1a).[41] Compound *E*-**1a** (0.15 g, yield 72%, mp 117–118 °C) was obtained from indanone **2a** (0.11 g, 0.57 mmol). ^{1}H NMR (600 MHz, CD$_3$OD): 7.74 (d, *J* = 8.1, 2H), 7.45 (s, 1H), 7.44 (d, *J* = 8.1, 2H), 7.24 (s, 1H), 7.13 (s, 1H), 3.95 (s, 3H), 3.92 (s, 2H), 3.87 (s, 3H), 3.64 (s, 2H), 2.57 (q, *J* = 7.2, 4H), 1.09 (t, *J* = 7.2, 6H). ^{13}C NMR (150 MHz, CD$_3$OD): 193.8, 156.2, 149.9, 146.1, 140.4, 135.3, 134.2, 132.0, 130.3, 130.2, 129.7, 107.4, 104.4, 56.7, 55.3, 55.0, 46.3, 31.6, 10.1. MS (ESI): *m/z* 366.2 (M + H$^+$).

(***Z***)-2-(4-((Diethylamino)methyl)benzylidene)-5,6-dimethoxy-2,3-dihydro-1*H*-inden-1-one (***Z***-1a). ^{1}H NMR (600 MHz, CD$_3$OD): 8.02 (d, *J* = 8.1, 2H), 7.34 (d, *J* = 8.1, 2H), 7.18 (s, 1H), 7.02 (s, 1H), 6.96 (s, 1H), 3.93 (s, 3H), 3.85 (s, 3H), 3.75 (s, 2H), 3.65 (s, 2H), 2.58 (q, *J* = 7.2, 4H), 1.10 (t, *J* = 7.1, 6H). ^{13}C NMR (150 MHz, CD$_3$OD): 191.6, 156.0, 149.8, 145.0, 139.6, 137.6, 135.3, 134.0, 133.0, 130.8, 128.7, 107.0, 104.3, 56.7, 55.3, 55.0, 46.3, 34.4, 10.0.

(***E***)-2-(4-((Diethylamino)methyl)benzylidene)-2,3-dihydro-1*H*-inden-1-one (***E***-1b). Compound *E*-**1b** (0.14 g, yield 83%, mp 82–84 °C) was obtained from indanone **2b** (0.073 g, 0.55 mmol). ^{1}H NMR (600 MHz, CD$_3$OD): 7.82 (d, *J* = 7.6, 1H), 7.72–7.63 (m, 3H), 7.65 (t, *J* = 7.1, 1H), 7.60 (s, 1H), 7.51–7.42 (m, 3H), 4.07 (s, 2H), 3.65 (s, 2H), 2.58 (q, *J* = 7.2, 4H), 1.09 (t, *J* = 7.2, 6H). ^{13}C NMR (150 MHz, CD$_3$OD): 195.0, 150.4, 140.7, 137.5, 134.8, 134.6, 134.1, 133.7, 130.6, 129.7, 127.5, 126.3, 123.6, 56.7, 46.4, 31.9, 10.1. MS(ESI): *m/z* 306.1 [M + H$^+$].

(***Z***)-2-(4-((Diethylamino)methyl)benzylidene)-2,3-dihydro-1*H*-inden-1-one (***Z***-1b). ^{1}H NMR (600 MHz, CD$_3$OD): 8.07 (d, *J* = 8.0, 2H), 7.76 (d, *J* = 7.6, 1H), 7.64 (m, 1H), 7.55 (d, *J* = 7.6, 1H), 7.43 (t, *J* = 7.5, 1H), 7.38 (d, *J* = 8.0, 2H), 7.11 (s, 1H), 3.92 (s, 2H), 3.65 (s, 2H), 2.59 (q, *J* = 7.1, 4H), 1.10 (t, *J* = 7.1, 6H). ^{13}C NMR (150 MHz, CD$_3$OD): 192.3, 149.3, 140.0, 139.3, 134.7, 134.4, 134.1, 133.9, 130.9, 128.8, 127.2, 125.9, 123.5, 56.7, 46.3, 34.7, 10.0.

(*E*)-2-(4-((Diethylamino)methyl)benzylidene)-5-methoxy-2,3-dihydro-1*H*-inden-1-one (*E*-1c). Compound *E*-1c (0.15 g, yield 81%, mp 106–107 °C) was obtained from indanone 2c (0.089 g, 0.55 mmol). ^{1}H NMR (600 MHz, CD$_3$OD): 7.75 (d, *J* = 8.5, 1H), 7.68 (d, *J* = 8.0, 2H), 7.52 (s, 1H), 7.47 (d, *J* = 8.0, 2H), 7.14 (s, 1H), 7.00 (dd, *J* = 8.4, 1.8, 1H), 4.02 (s, 2H), 3.92 (s, 3H), 3.69 (s, 2H), 2.61 (q, *J* = 7.1, 4H), 1.11 (t, *J* = 7.1, 6H). ^{13}C NMR (150 MHz, CD$_3$OD): 190.4, 166.1, 153.6, 139.9, 135.3, 134.4, 132.3, 130.6, 130.4, 129.8, 125.5, 115.5, 109.5, 56.6, 55.0, 46.4, 32.0, 10.0. MS(ESI): *m/z* 336.2 [M + H^{+}].

(*Z*)-2-(4-((Diethylamino)methyl)benzylidene)-5-methoxy-2,3-dihydro-1*H*-inden-1-one (*Z*-1c). ^{1}H NMR (600 MHz, CD$_3$OD): 8.04 (d, *J* = 8.1, 2H), 7.69 (d, *J* = 8.6, 1H), 7.37 (d, *J* = 8.1, 2H), 7.04 (s, 2H), 6.98 (dd, *J* = 8.5, 2.1, 1H), 3.90 (s, 2H), 3.86 (s, 3H), 3.70 (s, 2H), 2.63 (q, *J* = 7.2, 4H), 1.12 (t, *J* = 7.2, 6H). ^{13}C NMR (150 MHz, CD$_3$OD): 189.0, 165.7, 152.5, 137.9, 135.3, 134.3, 134.2, 133.4, 130.8, 128.8, 125.4, 115.5, 108.8, 56.6, 54.9, 46.3, 34.7, 9.8.

(*E*)-2-(4-((Diethylamino)methyl)benzylidene)-6-methoxy-2,3-dihydro-1*H*-inden-1-one (*E*-1d). Compound *E*-1d (0.14 g, yield 76%, mp 100.5–102 °C) was obtained from indanone 2d (0.089 g, 0.55 mmol). ^{1}H NMR (600 MHz, CD$_3$OD): 7.66 (d, *J* = 8.0, 2H), 7.55 (s, 1H), 7.51 (d, *J* = 8.3, 1H), 7.45 (d, *J* = 8.0, 2H), 7.27 (d, *J* = 2.2, 1H), 7.24 (dd, *J* = 8.3, 2.5, 1H), 3.95 (s, 2H), 3.84 (s, 3H), 3.62 (s, 2H), 2.56 (q, *J* = 7.1, 4H), 1.08 (t, *J* = 7.1, 6H). ^{13}C NMR (150 MHz, CD$_3$OD): 194.9, 159.8, 143.0, 140.9, 138.7, 135.4, 134.0, 133.5, 130.5, 129.7, 127.0, 123.5, 105.4, 56.7, 54.7, 46.3, 31.2, 10.2. MS(ESI): *m/z* 336.2 [M + H^{+}].

(*Z*)-2-(4-((Diethylamino)methyl)benzylidene)-6-methoxy-2,3-dihydro-1*H*-inden-1-one (*Z*-1d). ^{1}H NMR (600 MHz, CD$_3$OD): 8.07 (d, *J* = 8.1, 2H), 7.46 (d, *J* = 8.2, 1H), 7.37 (d, *J* = 8.1, 2H), 7.24 (m, 2H), 7.08 (s, 1H), 3.83 (s, 2H), 3.82 (s, 3H), 3.64 (s, 2H), 2.57 (q, *J* = 7.0, 4H), 1.10 (t, *J* = 7.1, 6H). ^{13}C NMR (150 MHz, CD$_3$OD): 192.4, 159.7, 142.0, 141.2, 140.0, 139.1, 135.3, 133.9, 130.8, 128.7, 126.7, 123.3, 105.1, 56.7, 54.6, 46.3, 34.0, 10.0.

Cholinesterases assays

Inhibition of human recombinant AChE (2770 U mg^{−1}) or BChE from human serum (50 U mg^{−1}; both from Sigma Aldrich), was determined as previously described, by applying the Ellman's spectrophotometric method to a 96-well plate procedure.[49]

MAO assays

Inhibition of human recombinant MAO A and B (Sigma-Aldrich Italy) was determined using an already described spectrofluorimetric method, based on the oxidative deamination of kynuramine to 4-hydroxyquinoline.[54] Samples were prepared in black, flat-bottomed 96-well plates (Greiner Bio-One, Kremsmenster, Austria) and spectrofluorimetric reads made with a multiplate reader Infinite M1000 Pro (Tecan, Cernusco sul Naviglio, Italy). IC$_{50}$ values were obtained by nonlinear regression using Prism software (GraphPad Prism version 5.01 for Windows, GraphPad Software, San Diego, CA, USA).

Inhibition of Aβ$_{40}$ aggregation

The spectrofluorimetric ThT fluorescence-based assay of Aβ aggregation was performed as previously described.[55] Samples were prepared in 96-well black, non-binding microplates (Greiner Bio-One GmbH, Frickenhausen, Germany) containing Aβ$_{40}$ (EZBiolab, Carmel, IN, USA) and inhibitors to a final concentration of 30 and 100 μM respectively in PBS (pH 7.4) containing 2% 1,1,1,3,3,3-hexafluoro-2-propanol (HFIP). After 2 h of incubation at 25 °C, 25 μM ThT solution was added and fluorescence was determined with a multi-plate reader Infinite M1000 Pro (Tecan, Cernusco S.N., Italy). Assays were carried out in triplicate and values are reported as mean ± SD.

RP-HPLC separation

The *E/Z* mixture of compound 1c has been separated on Agilent 1260 preparative binary pump HPLC apparatus, endowed of a DAD detector. The stationary phase was the preparative Phenomenex Synergi C8 Fusion-RP 10 μ (250 × 10 mm) column. The mixture was solubilized to a 0.5 mg mL^{−1} in methanol, and eluted (flow 5 mL min^{−1}) by a mobile phase constituted of ammonium formate (50 mM, pH 3.5)/methanol 1/1 v/v mixtures. The elution of compounds has been monitored at a wavelength of 330 nm.

After separation, the qualitative analyzes have been carried out on Agilent 1260 binary pump HPLC apparatus, and a Phenomenex Synergi C18 Fusion-RP 4 μ (150 × 4.6 mm) stationary phase, by eluting at flow 1 mL min^{−1}, with the mobile phase applied in the preparative separation (detection with DAD at 330 nm). The analytical chromatograms of *E* and *Z* isomers are reported in the ESI.†

Docking studies

Docking simulations were performed using the crystal structure of *h*AChE in complex with donepezil (PDB code 4EY7),[56] *h*MAO-B complexed with safinamide (PDB code 2V5Z)[57] and *h*MAO-A complexed with harmine (PDB code 2Z5X),[58] retrieved from the Protein Data Bank.[59] The protein pretreatment to remove water molecules, assign bond orders, add hydrogen atoms, create disulfide bonds, fill in missing side chains and loops using Prime[60] and cap termini was carried out with the Protein Preparation Wizard[61] module available from Schrödinger Release 2021-3. Protonation states at pH 7.0 ± 2.0 and tautomers for histidine residues were predicted with the Epik function and default parameters were used for the optimization of hydrogen-bond assignment. A restrained energy minimization step only on hydrogens was finally applied to the protein using the OPLS4 (ref. 62) force field. The ligand preparation was performed using the LigPrep module in the Schrödinger Suite. *E*-1c and *Z*-1c were initially drafted in the Maestro panel; then protonation states were calculated at pH 7.0 ± 2.0 retaining specific chiralities and applying the OPLS4 force field. The "Receptor Grid Generation" panel of Glide[63] was used to generate the grid files with grid points calculated within an enclosing box of

20 Å defined by the X-ray coordinates of donepezil and safinamide taken from 4EY7 and 2V5Z, respectively. Docking calculations were performed for each ligand using the Glide module of Schrödinger, using standard (SP) mode and default settings (van der Waals radius scaling parameters: scaling factor of 0.80 and partial charge cut-off of 0.15; dock flexibly; add Epik state penalties to docking score; perform post-docking minimization). The scoring function of Glide known as "Docking score" was used for estimating the binding affinity. Pictures were elaborated with Schrödinger.

Author contributions

Conceptualization, M. P., F. C., C. D. A.; formal analysis, M. P., S. M., M. R., M. d. C., L. P., M. C.; Investigation, M. P., S. M., M. R., M. d. C., L. P., M. C., C. M., A. B., A. C., M. O.; project administration, M. P., F. C., C. D. A.; writing – original draft M. P., S. M., M. R., M. d. C., L. P., M. C., C. M., A. B., A. C., M. O., F. C., C. D. A.

Conflicts of interest

There are no conflicts to declare.

Acknowledgements

Notes and references

1 K. Gerrow and A. Triller, *Curr. Opin. Neurobiol.*, 2010, **20**, 631–639.

2 S. E. Hyman, *Curr. Biol.*, 2005, **15**, R154–R158.

3 M. R. Picciotto, M. J. Higley and Y. S. Mineur, *Neuron*, 2012, **76**, 116–129.

4 M. Racchi, M. Mazzucchelli, E. Porrello, C. Lanni and S. Govoni, *Pharmacol. Res.*, 2004, **50**, 441–451.

5 A. J. Wagstaff and D. McTavish, *Drugs Aging*, 1994, **4**, 510–540.

6 S. A. Eagger, R. Levy and B. J. Sahakian, *Lancet*, 1991, **337**, 989–992.

7 C. M. Spencer and S. Noble, *Drugs Aging*, 1998, **13**, 391–411.

8 L. Maggi and R. Mantegazza, *Clin. Drug Invest*, 2011, **31**, 691–701.

Q7 9 N. Kunzler and T. B. Erickson, in *History of Toxicology and Environmental Health*, ed. A. D. B. T.-H. of M. C. T. Woolf, Academic Press, 2022, pp. 271–278.

10 M. Dooley and H. M. Lamb, *Drugs Aging*, 2000, **16**, 199–226.

11 Z. Cai, *Mol. Med. Rep.*, 2014, **9**, 1533–1541.

12 S. Carradori and R. Silvestri, *J. Med. Chem.*, 2015, **58**, 6717–6732.

13 J. P. M. Finberg and J. M. Rabey, *Front. Pharmacol.*, 2016, **7**, 340.

14 B. Kumar, Sheetal, A. K. Mantha and V. Kumar, *RSC Adv.*, Q8 2016, **6**, 42660–42683.

15 E. Cereda, R. Cilia, M. Canesi, S. Tesei, C. B. Mariani, A. L. Zecchinelli and G. Pezzoli, *J. Neurol.*, 2017, **264**, 1254–1263.

16 F. Chimenti, R. Fioravanti, A. Bolasco, P. Chimenti, D. Secci, F. Rossi, M. Yáñez, F. Orallo, F. Ortuso and S. Alcaro, *J. Med. Chem.*, 2009, **52**, 2818–2824.

17 M. S. Nel, A. Petzer, J. P. Petzer and L. J. Legoabe, *Bioorg. Med. Chem. Lett.*, 2016, **26**, 4599–4605.

18 L. Huang, C. Lu, Y. Sun, F. Mao, Z. Luo, T. Su, H. Jiang, W. Shan and X. Li, *J. Med. Chem.*, 2012, **55**, 8483–8492.

19 S. Maramai, M. Benchekroun, M. T. Gabr and S. Yahiaoui, *BioMed Res. Int*, 2020, **2020**, 5120230.

20 J. Sterling, Y. Herzig, T. Goren, N. Finkelstein, D. Lerner, W. Goldenberg, I. Miskolczi, S. Molnar, F. Rantal, T. Tamas, G. Toth, A. Zagyva, A. Zekany, G. Lavian, A. Gross, R. Friedman, M. Razin, W. Huang, B. Krais, M. Chorev, M. B. Youdim and M. Weinstock, *J. Med. Chem.*, 2002, **45**, 5260–5279.

21 B. Mathew, J. M. Oh, R. S. Baty, G. E.-S. Batiha, D. G. T. Parambi, N. Gambacorta, O. Nicolotti and H. Kim, *Environ. Sci. Pollut. Res.*, 2021, **28**, 38855–38866.

22 Q. He, J. Liu, J.-S. Lan, J. Ding, Y. Sun, Y. Fang, N. Jiang, Z. Yang, L. Sun, Y. Jin and S.-S. Xie, *Bioorg. Chem.*, 2018, **81**, 512–528.

23 R. R. Ramsay, M. R. Popovic-Nikolic, K. Nikolic, E. Uliassi and M. L. Bolognesi, *Clin. Transl. Med.*, 2018, **7**, 3.

24 W. A. Velema, W. Szymanski and B. L. Feringa, *J. Am. Chem. Soc.*, 2014, **136**, 2178–2191.

25 M. J. Fuchter, *J. Med. Chem.*, 2020, **63**, 11436–11447.

26 A. Duran-Corbera, J. Catena, M. Otero-Viñas, A. Llebaria and X. Rovira, *J. Med. Chem.*, 2020, **63**, 8458–8470.

27 D. A. Rodríguez-Soacha, J. Fender, Y. A. Ramírez, J. A. Collado, E. Muñoz, R. Maitra, C. Sotriffer, K. Lorenz and M. Decker, *ACS Chem. Neurosci.*, 2021, **12**, 1632–1647.

28 Z. Qiao, W. Fu, Y. Zhang, R. Chen, Z. Xu, Z. Li and X. Shao, *J. Agric. Food Chem.*, 2021, **69**, 15554–15561.

29 L. Yue, M. Pawlowski, S. S. Dellal, A. Xie, F. Feng, T. S. Otis, K. S. Bruzik, H. Qian and D. R. Pepperberg, *Nat. Commun.*, 2012, **3**, 1095.

30 A. Mourot, M. A. Kienzler, M. R. Banghart, T. Fehrentz, F. M. E. Huber, M. Stein, R. H. Kramer and D. Trauner, *ACS Chem. Neurosci.*, 2011, **2**, 536–543.

31 W. Szymanski, M. E. Ourailidou, W. A. Velema, F. J. Dekker and B. L. Feringa, *Chem. – Eur. J.*, 2015, **21**, 16517–16524.

32 B. Reisinger, N. Kuzmanovic, P. Löffler, R. Merkl, B. König and R. Sterner, *Angew. Chem., Int. Ed.*, 2014, **53**, 595–598.

33 X. Rovira, A. Trapero, S. Pittolo, C. Zussy, A. Faucherre, C. Jopling, J. Giraldo, J.-P. Pin, P. Gorostiza, C. Goudet and A. Llebaria, *Cell Chem. Biol.*, 2016, **23**, 929–934.

34 X. Chen, S. Wehle, N. Kuzmanovic, B. Merget, U. Holzgrabe, B. König, C. A. Sotriffer and M. Decker, *ACS Chem. Neurosci.*, 2014, **5**, 377–389.

35 J. Broichhagen, I. Jurastow, K. Iwan, W. Kummer and D. Trauner, *Angew. Chem., Int. Ed.*, 2014, **53**, 7657–7660.

36 M. Scheiner, A. Sink, M. Hoffmann, C. Vrigneau, E. Endres, A. Carles, C. Sotriffer, T. Maurice and M. Decker, *J. Am. Chem. Soc.*, 2022, **144**, 3279–3284.

37 M. Scheiner, A. Sink, P. Spatz, E. Endres and M. Decker, *ChemPhotoChem*, 2021, **5**, 149–159.

38 M. Paolino, M. Gueye, E. Pieri, M. Manathunga, S. Fusi, A. Cappelli, L. Latterini, D. Pannacci, M. Filatov, J. Léonard and M. Olivucci, *J. Am. Chem. Soc.*, 2016, **138**, 9807–9825.

39 M. Paolino, T. Giovannini, M. Manathunga, L. Latterini, G. Zampini, R. Pierron, J. Léonard, S. Fusi, G. Giorgi, G. Giuliani, A. Cappelli, C. Cappelli and M. Olivucci, *J. Phys. Chem. Lett.*, 2021, **12**, 3875–3884.

40 G. Tassone, M. Paolino, C. Pozzi, A. Reale, L. Salvini, G. Giorgi, M. Orlandini, F. Galvagni, S. Mangani, X. Yang, B. Carlotti, F. Ortica, L. Latterini, M. Olivucci and A. Cappelli, *ChemBioChem*, 2022, **23**, e202100449.

41 R. Sheng, Y. Xu, C. Hu, J. Zhang, X. Lin, J. Li, B. Yang, Q. He and Y. Hu, *Eur. J. Med. Chem.*, 2009, **44**, 7–17.

Q9 42 CN1709860A20051221, 2005, pp. 1–23.

43 N. Chitranshi, S. Gupta, P. K. Tripathi and P. K. Seth, *Med. Chem. Res.*, 2013, **22**, 2328–2345.

44 L. Shen, G. Liu and Y. Tang, *Acta Pharmacol. Sin.*, 2007, **28**, 2053–2063.

45 S. Akhilesh, M. Anurag, P. Ram Prakash, J. Suresh and B. Anil, *J. Chem. Pharm. Res.*, 2010, **2**, 682–689.

46 A. Affini, S. Hagenow, A. Zivkovic, J. Marco-Contelles and H. Stark, *Eur. J. Med. Chem.*, 2018, **148**, 487–497.

47 M. L. Salum, P. Arroyo Mañez, F. J. Luque and R. Erra-Balsells, *J. Photochem. Photobiol., B*, 2015, **148**, 128–135.

48 P. Perjési, M. Takács, E. Ösz, Z. Pintér, J. Vámos and K. Takács-Novák, *J. Chromatogr. Sci.*, 2005, **43**, 289–295.

49 R. Purgatorio, M. de Candia, M. Catto, A. Carrieri, L. Pisani, A. De Palma, M. Toma, O. A. Ivanova, L. G. Voskressensky and C. D. Altomare, *Eur. J. Med. Chem.*, 2019, **177**, 414–424.

50 R. Purgatorio, M. de Candia, M. Catto, M. Rullo, L. Pisani, N. Denora, A. Carrieri, A. A. Nevskaya, L. G. Voskressensky and C. D. Altomare, *ChemMedChem*, 2021, **16**, 589–598.

51 E. McDade, *J. Am. Geriatr. Soc.*, 2019, **67**, 845–847.

52 R. Purgatorio, M. De Candia, A. De Palma, F. De Santis, L. Pisani, F. Campagna, S. Cellamare, C. D. Altomare and M. Catto, *Molecule*, 2018, **23**, 1544.

53 S. Gemma, G. Kukreja, C. Fattorusso, M. Persico, M. P. Romano, M. Altarelli, L. Savini, G. Campiani, E. Fattorusso, N. Basilico, D. Taramelli, V. Yardley and S. Butini, *Bioorg. Med. Chem. Lett.*, 2006, **16**, 5384–5388.

54 L. Pisani, R. M. Iacobazzi, M. Catto, M. Rullo, R. Farina, N. Denora, S. Cellamare and C. D. Altomare, *Eur. J. Med. Chem.*, 2019, **161**, 292–309.

55 R. Purgatorio, L. N. Kulikova, L. Pisani, M. Catto, M. de Candia, A. Carrieri, S. Cellamare, A. De Palma, A. A. Beloglazkin, G. Reza Raesi, L. G. Voskressensky and C. D. Altomare, *ChemMedChem*, 2020, **15**, 1947–1955.

56 J. Cheung, M. J. Rudolph, F. Burshteyn, M. S. Cassidy, E. N. Gary, J. Love, M. C. Franklin and J. J. Height, *J. Med. Chem.*, 2012, **55**, 10282–10286.

57 C. Binda, J. Wang, L. Pisani, C. Caccia, A. Carotti, P. Salvati, D. E. Edmondson and A. Mattevi, *J. Med. Chem.*, 2007, **50**, 5848–5852.

58 S. Se-Young, M. Jichun, K. Youhei, Y. Masato, Y. Eiki and T. Tomitake, *Proc. Natl. Acad. Sci. U. S. A.*, 2008, **105**, 5739–5744.

59 https://www.rcsb.org/. Q10

60 M. P. Jacobson, R. A. Friesner, Z. Xiang and B. Honig, *J. Mol. Biol.*, 2002, **320**, 597–608.

61 G. Madhavi Sastry, M. Adzhigirey, T. Day, R. Annabhimoju and W. Sherman, *J. Comput.-Aided Mol. Des.*, 2013, **27**, 221–234.

62 C. Lu, C. Wu, D. Ghoreishi, W. Chen, L. Wang, W. Damm, G. A. Ross, M. K. Dahlgren, E. Russell, C. D. Von Bargen, R. Abel, R. A. Friesner and E. D. Harder, *J. Chem. Theory Comput.*, 2021, **17**, 4291–4300.

63 R. A. Friesner, R. B. Murphy, M. P. Repasky, L. L. Frye, J. R. Greenwood, T. A. Halgren, P. C. Sanschagrin and D. T. Mainz, *J. Med. Chem.*, 2006, **49**, 6177–6196.